CLM-R179

CLM-R179

UKAEA

Report

THE DITE TOKAMAK MULTI-PULSE THOMSON SCATTERING SYSTEM

R PRENTICE

CULHAM LABORATORY
Abingdon Oxfordshire

1978

Available from H. M. Stationery Office

C/18

£1.50

CLM-R 179

THE DITE TOKAMAK MULTI-PULSE THOMSON SCATTERING SYSTEM

R. Prentice

Culham Laboratory, Abingdon, Oxon, OX14 3DB, UK
(Euratom/UKAEA Fusion Association)

A B S T R A C T

A four pulse ruby laser scattering system for measuring electron temperature and density in a tokamak plasma is discussed in detail. It is shown that the divergence of the laser has to be adequately controlled. By using notch filters to eliminate the stray laser light, instead of baffles, measurements can be performed at any position over a large fraction of the minor diameter of the plasma. The transmission of the detecting system was optimised using a computer ray tracing programme. Results from the apparatus are shown to be in substantial agreement with those obtained using other techniques.

May 1978

KS

SBN: 85311 065 4

INTRODUCTION

One of the most important parameters specifying a plasma is the electron temperature. Descriptions of phenomena such as power and energy balance, transport processes and spectroscopic rate coefficients all depend on knowledge of the electron temperature as a function of space and time. Before the advent of scattering techniques, the electron temperature of highly energetic plasmas was deduced from measurements on the emitted X-ray spectrum[1], microwave noise[2], the plasma diamagnetism[3] or by spectroscopy techniques[4]. All of these methods suffered from a lack of accurate spatial resolution and, in the case of the latter two, depend on a knowledge of plasma parameters other than the electron temperature. The Thomson scattering technique employing a giant pulsed laser overcame these drawbacks by measuring directly the electron temperature within a small volume ($\leq 0.1\,cm^3$) at a well defined time ($\leq$ 100 ns).

The scattering technique exploits the basic principle that monochromatic photons, directed through a plasma, can be scattered from free moving electrons and therefore frequency shifted by the Doppler effect. Wavelength analysis of the scattered photons will then yield information on the electrons' motion and hence temperature. The difficulty with this technique rests in the fact that the relevant, Thomson cross-section is very small ($6.65 \times 10^{-29}\ m^2$), with the result that a negligible

number of scattered photons would be produced if the plasma were illuminated with a conventional light source. Application of the technique was not therefore possible until lasers, and in particular ruby lasers, with extremely intense well collimated beams became available.

The early work and general considerations for scattering experiments have been reviewed in both papers and books[5,6,7].

The first application of the technique to the relatively low density plasma in a tokamak was performed on the T3-A[8] tokamak at the Kurchatov Institute, Moscow. This experiment clearly demonstrated the viability of the method for a tokamak plasma. Values of temperature and density were measured over a wide range and these were shown to agree with results obtained from other diagnostics.

For DITE tokamak[9] the system was designed to utilise a four pulse ruby laser, so that the temperature could be measured several times in a single machine pulse. The scattering angle is 90^{o}, and the scan of the plasma is achieved by moving the entire system in the horizontal plane. This contrasts with the T3-A system in which the vertical laser beam was fixed and the collection optics system viewed different points along its length.

PRINCIPLES AND ESTIMATES OF SIGNAL MAGNITUDES

The nature of the scattering of electromagnetic radiation by a plasma is largely determined by the parameter, α, defined by the relationship:

$$\alpha = \frac{\lambda_L}{4\pi \lambda_D \sin(\theta/2)} \qquad \ldots\ (1)$$

where λ_L is the wavelength of the incident radiation, in this case 6943 Å for the ruby laser; θ is the scattering angle, 90^{o} for this case;

$\lambda_D = 743\sqrt{\frac{T_e\ (eV)}{n_e(cm^3)}}$ cm, is the Debye length, and T_e, n_e are the electron temperature and density respectively. For the scattering to be independent of collective effects and therefore to be uniquely determined by the electron energy distribution function, we need $\alpha \lesssim 0.1$[5]. For this condition to be met with this apparatus we derive the following inequality:

$$\frac{T_e}{n_e} > 1.1 \times 10^{-14}\ \text{eV cm}^3. \qquad \ldots\ (2)$$

This condition is easily satisfied for normal tokamak conditions with $T_e > 10$ eV and $n_e < 5 \times 10^{14}$ cm^{-3}.

When the temperature of the plasma is low, the form of the intensity distribution of the scattered light is determined by the Doppler effect associated with the thermal motion of the electrons. The spectral profile is then a simple Gaussian with its peak intensity at the wavelength of the laser and a characteristic half width at half maximum given by:

$$\Delta\lambda_G = 16.2\sqrt{T_e\ (eV)}\ \text{Å}. \qquad \ldots\ (3)$$

If the temperature is relatively high ($\gtrsim$ 1 keV) then the relativistic effects of high energy electrons in the tail of the velocity distribution have to be taken into account. The form of the profile is then described by the relationship[10]

$$P_{sc}\ (\lambda_s)\ d\Omega\ d\lambda_s = \frac{P_L\ r_o^2\ n_e\ cL}{a\ \lambda_L\ (2\pi)^{\frac{1}{2}}}\ f(x)\ \exp\left\{-\left(\frac{c}{a}\right)^2 Z(x)\right\}\ d\Omega\ d\lambda_s \qquad \ldots\ (4)$$

where $x = (\lambda_s - \lambda_L)/\lambda_L$

$f(x) = 1 - 3.5\ x + 7.6\ x^2 - 13.3\ x^3$

$Z(x) = x^2\ (1 - x)/2$

λ_s = Wavelength of scattered light

$a^2 = 2\ kT_e/m_e$.

r_o = Classical radius of the electron

c = Velocity of light

L = Length of the laser beam viewed

P_L = Input power of the ruby laser

$P_{sc}(\lambda_s)$ = Power scattered per unit solid angle per unit wavelength interval.

From equation (4) it can be seen that the peak of the profile is no longer at the laser wavelength, but has been shifted to a slightly shorter wavelength. In addition, the profile is no longer symmetric about its peak value.

Experimental Considerations

For convenience, the experimental method can be regarded as a number of separate operations. Briefly, these operations are as follows. The laser beam is directed and focussed through a small volume of plasma called the scattering volume. A sample of the scattered light from this volume is collected and then dispersed in a polychromator. The output signals from the polychromator, at several wavelengths, are first converted to electrical signals, then digitised and are finally transferred to a computer. The latter fits equation (4) to the measured data by varying n_e and T_e independently, in a routine that minimises the statistical parameter χ^2.

Scattered Photons

In order to demonstrate the feasibility of the experiment we need to show that signals can be obtained from the detectors which are sufficiently large to have reasonable statistics and are also large enough to overcome the signals due to plasma radiation and stray light

from the laser, if the latter is present.

We deal first with the magnitude of the scattered signals. For convenience we assume that the scattered profile is Gaussian, which means that equation (4) can be simplified:

$$f(x) \rightarrow 1$$

and $$Z(x) \rightarrow x^2/2.$$

Finally, equation (4) can be adapted to yield:

$$n_s = 1.16 \times 10^{-12} E_L(J)\, n_e(cm^{-3})\, L(cm)\, \lambda_s(\mathring{A})\, \Omega(Ster)\, W(\mathring{A})\, T_e^{-\frac{1}{2}}\ (eV)$$

$$\exp\left(-2.65 \times 10^{-3} \Delta\lambda^2\, T_e^{-1}\right) \text{ photons} \qquad \ldots. (5)$$

where E_L = Laser energy

Ω = Solid angle subtended at the scattering volume by the objective lens

W = Width of each polychromator channel

$\Delta\lambda = \lambda_s - \lambda_L\ (\mathring{A})$.

We also arrange to utilize only the light on the short wavelength side of the laser line since, in this region, the decreasing intensity of the scattered light is counteracted by increasing sensitivity of the detectors (photomultipliers), whilst on the long wavelength side both the intensity and sensitivity decrease with increasing wavelength.

Before DITE commenced operation a typical value for the electron temperature of the plasma was considered to be 400 eV. In order to measure such a temperature with reasonable accuracy we decide to split the spectral profile into say 10 channels, which is a compromise between resolution and complexity plus expense. The bandwidth of each channel is then fixed so that the outermost channel has an intensity of about 10% of the innermost channel. This leads to the condition:

$$W = \Delta\lambda_G/5$$

where W (Å) is the width of each channel. The edge of the first channel was then arranged to be coincident with the edge of the laser line. We therefore deduce that W = 64.8 Å and hence:

$$\Delta\lambda_1 = 64.8 \text{ Å} \qquad \Delta\lambda_{10} = 648 \text{ Å}$$

$$\lambda_{s_1} = 6878.2 \text{ Å} \qquad \lambda_{s_{10}} = 6295 \text{ Å}$$

Using these values in turn in equation (5), together with the following values for the other variables: E_L = 5 J through the scattering volume, $n_e = 2 \times 10^{13}$ cm^{-3}; L = 1 cm, Ω = 0.02 Ster (f/6 system partially shadowed by a 50 mm wide slot) yields the number of photons collected by the objective lens for the best (1st) and worst (10th) channels:

$$n_{s_1} = 50{,}400 \quad ; \quad n_{s_{10}} = 2{,}900 \text{ photons} \qquad \ldots\ (6)$$

Plasma Photons

As well as scattered photons, the system will also collect those due to plasma radiation. An important source of plasma radiation is bremsstrahlung, generated when electrons undergo free-free transitions in the Coulomb fields of plasma ions. The rate of bremsstrahlung radiation in the visible spectrum is given by the following equation[11]:

$$\rho_\omega(\omega,T_e) = \left(\frac{16}{3}\right)\left(\frac{2\pi}{3}\right)^{\frac{1}{2}}\left(\frac{e^2}{4\pi\,\varepsilon_o C\sqrt{m_e}}\right)^3 \frac{n_e n_i Z^2}{(kT_e)^{\frac{1}{2}}}\,\bar{G}(\omega,T_e)\exp\left(\frac{-\hbar\omega}{kT_e}\right)d\omega \text{ W m}^{-3} \qquad \ldots\ (7)$$

where $\bar{G}(\omega,T)$ is the Gaunt factor averaged over the Maxwellian distribution, n_i is the density of ions with charged state Z and the fundamental constants have their appropriate values. Again, equation (7) can be adapted to a more suitable form:

$$n_p = 7.62 \times 10^{-15}\left(\frac{n_e n_i Z^2}{\lambda_s T_e^{\frac{1}{2}}}\right)\bar{G}\,V_p\,\Omega\exp\left(\frac{-\varepsilon_\nu}{kT_e}\right)\tau\,d\lambda_s \text{ Photons} \qquad \ldots\ (8)$$

where V_p is the effective volume of plasma radiating into the solid

angle Ω, ε_ν is the photon energy, τ is the gating time for the signals and $d\lambda_s$ is the appropriate wavelength interval. If we make the assumption that the plasma is purely hydrogenic then $n_e = n_i$ and $Z = 1$. For our case ε_ν/kT is $\approx$ 0.005, which means that the exponential term is very close to 1. This value for ε_ν/kT can also be used to determine the appropriate value of $\bar{G}$ (≈ 3) from published data on Gaunt factors[12]. It has been shown[6] that the value of V_p is given by the cross-sectional area of the image of the polychromator slit, at the position of the scattering volume, multiplied by the full width of the plasma; thus $V_p = 13\ cm^3$. A sufficient value for τ is 100 ns in order to straddle all the photomultiplier signals. Using the above figures together with those used previously we can estimate the number of photons in the 1st and 10th channels:

$$n_{p_1} = 112 \quad ; \quad n_{p_{10}} = 122 \text{ photons.}$$

There are two effects which will modify these values; firstly, experiment on a tokamak[8] has shown that equation (8) underestimates plasma radiation by a factor of perhaps 200, due almost certainly to impurity radiation, and secondly, because the useful scattered light will be plane polarized, an efficient polarizing element can be used in the system to halve the level of plasma light. Combining these two effects we estimate the effective values for the photon emission from the plasma to be approximately:

$$n_{p_1} = 11{,}200 \quad ; \quad n_{p_{10}} = 12{,}200 \text{ photons} \quad .... (9)$$

Photoelectron Signals, Noise Levels and ADC Signals

The overall transmission of the optical system will only be about 0.1 and the quantum efficiency of the photocathode of the photomultiplier will be $\sim$ 0.075 at 6878 Å and $\sim$ 0.105 at 6295 Å. Thus the

number of photoelectrons produced for each of the signals in (6) and (9) will be

$$\left.\begin{array}{ll} n_{s_1}\ (e) = 378 & n_{s_{10}}\ (e) = 30 \\ n_{p_1}\ (e) = 84 & n_{p_{10}}\ (e) = 128 \end{array}\right\} \text{Photoelectrons} \quad \ldots (10)$$

The S/N ratio will be given by the ratio of the scattered photoelectrons to the fluctuations in the level of the plasma photoelectrons. The Poisson distribution will govern the statistics associated with these signals, with the result that the following S/N ratios apply:

$$\begin{array}{ll} (S/N)_1 = 378/84^{\frac{1}{2}} & (S/N)_{10} = 30/128^{\frac{1}{2}} \\ (S/N)_1 = 41{:}1 & (S/N)_{10} = 2.7{:}1 \end{array} \quad \ldots (11)$$

Thus the S/N ratio on the outermost channel appears to be satisfactory as well as that for the inner.

If the overall gain of a photomultiplier is G, then the total charge, q, produced at the anode due to n_{pe} photoelectrons leaving the photocathode will be:

$$q = e\ G\ n_{pe},$$

and if this charge is measured on a combined gated integrator and A.D.C. with a sensitivity S (Coulombs/count) then the number of counts, C, produced will be:

$$C = \frac{e\ G\ n_{pe}}{S}. \quad \ldots (12)$$

For our case $G \sim 10^6$; S = 0.4 pC/count. The number of counts produced by the photoelectron signals from (10) will be:

$$C_{s_1} = 151 \qquad C_{s_{10}} = 12 \quad \text{Counts} \quad \ldots (13)$$

The figures derived above are summarized in Table 1.

Thus the feasibility of a well designed system has been demonstrated and the only other condition which must be met is that a technique needs to be found for keeping the stray light level from the laser below

a few counts per channel. This objective is achieved by the use of two "notch" filters (described later) in tandem in the collection optics system.

Density Calibration

We also note in equation (4) that the signal at any value of λ_s is directly proportional to n_e, so that a radial profile of relative density can be obtained directly, so long as shot to shot variations in the output of the laser are taken into account. In addition, absolute values for the density can be derived if the complete system has been calibrated absolutely.

Limitations of the Experiment

The polychromator has a fixed bandwidth which will limit the range of temperatures which can be measured with reasonable accuracy. For high temperatures the ratio of the signals between the inner and outer channels (which crudely determines the temperature) will be small and this will give rise to a relatively large uncertainty in the temperature. Also, under these circumstances, the characteristic width of the profile will be comparable with the total bandwidth of the polychromator so that a significant fraction of the scattered photons will not be utilized. This will also increase the uncertainty in the measurement due to poorer photon statistics. When the temperature is very low only the innermost channels will be illuminated and there will be steep intensity gradients across these channels. This means that the central wavelength of the channel will no longer be the accurate value to use in the analysis routine, with the result that a systematic error will be generated. These effects, due to the fixed bandwidth, can be overcome by changing the grating, but this would be inconvenient during an experimental run because the system would have to be recalibrated.

As the electron density decreases fewer scattered photons will be received and this means that there will be an increase in the statistical uncertainties associated with each signal. These will lead indirectly, through the statistical weightings in the fitting routine, to an increase in the uncertainty associated with the temperature.

From the above discussion it is clear that the dominant experimental errors will be due to photo-electron statistics.

APPARATUS

General Specification

The main requirements placed on the apparatus are listed below:

1. The system should work reliably for say 1000 shots without re-alignment. When checks on alignment and calibration do become necessary they should be easily performed tasks taking the minimum of time.
2. In order to facilitate the production of accurate profiles it should be possible to scan the apparatus to any position on a minor diameter of the plasma, preferably without having to adjust any optical components.
3. On the DITE experiment it is possible to adjust the major diameter of the plasma, which is in the horizontal plane, and therefore the scattering volume must be capable of following these alterations in the major diameter if the central temperature is to be measured.
4. If possible, the laser should produce more than one giant pulse per plasma pulse so that the time development of profiles can be obtained from the minimum number of machine pulses. For many reasons it would also be desirable to produce a system which could measure an entire temperature profile in one shot. However, experience at Princeton[13] has shown that such a system is optically and mechanically complex.

5. Analogue signals from the system should be fed to an automatic data processing system which is capable of producing profiles of temperature and density between machine pulses.

Description of System

From the above considerations it was decided to design the experiment so that all of the optical apparatus, laser rail and detection equipment would be mounted on a trolley which was itself on a railway. A horizontal scan would be achieved by driving the trolley along the railway; during this process no part of the optical system would be manipulated. This design necessitates a long horizontal slot on both the top and bottom of the DITE vacuum vessel.

An advantage of this design is that checks on alignment, between the focused laser beam and the axis of the collection system, and intensity calibrations can be readily achieved, without disturbing the system, by moving the trolley to the back of the railway and then mounting the calibration apparatus on the exposed railway between the scattering system and the DITE load assembly.

General Design

A general view of the apparatus is shown in Figure 1. The laser rail is located on three adjustable support points (cone, groove and plane) which are themselves mounted on horizontal slides. The inclination and position of the laser can therefore be readily and accurately changed in any direction. The prism used to direct and focus the laser beam is situated at the end of the rectangular tube, which has been given the largest possible depth of section for maximum rigidity. This tube contains no apertures or any divergence limiter. The laser beam is dumped below the lower radial slot of the vacuum module in a trough dump. The lower, blue glass plate of this dump runs

continuously for the whole length of the slot and is set at the Brewster angle. The collection optics and the f/6 polychromator are located on the lower plate of the trolley and are totally enclosed to exclude ambient light and dust. A bank of 10 electrostatically and magnetically screened photomultipliers are slung immediately below the polychromator. A fibre optic lead is used to transmit the optical signal from each channel of the polychromator to each photomultiplier. Signals from the photomultipliers are led to a CAMAC system where they are digitised by a gated integrator and stored locally until a few seconds after the machine pulse. The stored numbers are then passed to the central ICL 470 computer via a local CTL MOD 1 computer. After analysis by the central computer the results are returned to a VDU and hardcopy unit, again via the MOD 1. This arrangement of the MOD 1 and 470 is part of the Culham Integrated Data Acquisition system[14].

Laser

The ruby laser system was manufactured by Apollo Lasers and is capable of producing four 10 J, ~ 25 ns pulses in a rapid burst. The temporal spacing between each pulse is independently and continuously variable, within 1 μs resolution, from 0.5 ms → 1000 ms. There are four capacitor banks, each with its own switching and pulse shaping circuitry, for both the amplifier and oscillator sections. The four pulses are produced by discharging the capacitor banks, in sequence, through both the oscillator and amplifier flashlamps. The Pockels cell is also pulsed on four occasions, at the appropriate instants during the flashlamp pulses. The system is in addition capable of producing two pulses, whose interpulse spacing is in the range 1 → 500 μs, by firing the Pockels cell circuit twice within the period of one flash-lamp pulse. This sequence can be repeated once, after a delay in the

range 0.5 ms → 1000 ms, by firing the Pockels cell twice more within a second flashlamp pulse. When operating in the latter mode the total energy will in general only be ~ 10 J within one flashlamp period, unless there is time between the Pockels cell pulses for the ruby rods to be significantly repumped.

The most significant problem associated with multi-pulsing the laser as described above is that of increased divergence for the 2nd, 3rd and 4th pulses. During the flashlamp pulse, heat is deposited in the ruby rod and it will be lost by radial conduction to the water around the rod on a time scale comparable with the interpulse separation. This process produces a radial temperature gradient and, since the refractive index is a function of temperature, a corresponding radial refractive index gradient. Wave-fronts traversing the length of the rod will then be distorted by the index gradient.

The laser heads in the oscillator and amplifier sections are identical and are fitted with 6" × $\frac{5}{8}$" diameter ruby rods. As delivered the full aperture of each rod was exploited, but tests using the apparatus shown in Fig. 2 showed that when the interpulse spacing was ~ 100 ms (near the worst condition) the system did not operate with sufficiently low divergence on all four pulses. This problem was overcome by restricting the aperture of the oscillator to ~ $\frac{5}{16}$" and then expanding the beam by ~×2 before entry to the amplifier. A second beam expander (~ × 2) was fitted immediately after the amplifier head and it was found necessary to set the spacing between the elements of this expander to be somewhat greater than for the standard 'parallel beam in - parallel beam out' condition. This increased spacing has the overall effect of making the beam expander a slightly positive element, which yields the best compromise over the four pulses. The results from the tests in which the spacing of the

2nd beam expander was varied are shown in Fig. 3. These indicate that finally ~ 90% of the energy in each of the four pulses could be focussed through a 2.5 mm diameter aperture when the latter was placed at the focus of a 66 cm focal length lens. This arrangement simulates quite accurately the situation in the actual experiment in which the focusing element has a focal length of ~ 66 cm and the design figure for the diameter of the scattering volume was 2.5 mm. The divergence of the output beam from the laser under these conditions is 3.8 mrad (full angle, 90% energy).

The final arrangement of the optical components on the laser rail is shown in Fig. 4.

Focusing of the laser beam is performed by a 45^{o} - 90^{o} - 45^{o} spectrosil prism, the input surface of which is convex. This prism is adjustable in a horizontal direction, and can also be rotated with high accuracy about a horizontal axis, which is coincident with the laser axis, so that the scattering volume can be accurately aligned with the optic axis of the collection optics system.

Collection and Filter Optics

The primary tasks of this section are to collect, from the scattering volume, a sufficient amount of light to fill the optics of the polychromator, to transmit this light with minimum loss and aberrations to the slit of the polychromator, and to reduce stray laser light to negligible levels. A schematic of the system is shown in Fig. 5.

The lens system itself consists of four elements. A large (100 mm diameter) lens, A, collects the light from the scattering volume and forms an aerial image of the scattering volume at the position of lens B. This second lens is a field lens and its function is to image lens A on the third lens C, and thus ensure that all rays continue through the system. Lenses C and D are held close together

in one mount and effectively form a doublet; the purpose of which is to relay the image from position B to the entrance slit of the polychromator. Lens D has negative power, but is less powerful than C, and its purpose is to reduce to a very low level the spherical aberrations caused by lenses A, B and C. A, B and C were made from high index glass (LaK10, n = 1.72) to reduce the level of spherical aberrations, whilst lens D was made from low index glass (BSC1, n = 1.51).

Using a relatively primitive ray tracing programme, meridional rays only were traced through the system. The radii of curvature of the surfaces of lens D were adjusted, whilst its power was kept constant, until spherical aberrations at the final image plane were at a minimum. No attempt was made to correct for chromatic aberrations. A much more sophisticated ray tracing programme, written by Celia Wilson and Andrew Riley of Culham, which allows skew rays to be traced through an optical system, has become available since the lens system under consideration here was designed. Results obtained using this program have shown that the residual chromatic aberrations offset to some extent the very effective corrections for spherical aberrations. However, the present system has about half the losses of a simple system, designed with Gaussian formulae, and only one glass type.

The level of stray laser light is significantly reduced by using two 'notch filters' which are positioned symmetrically with respect to the field lens. These filters have a passband characteristic such that the useful scattered light is reflected from the dielectric stack, whilst the laser light passes through and is dumped in a blue glass plate cemented to the back of the filter. In order to achieve a high rejection ratio it is necessary to have a very high transmission ($\sim$ 90%) for the laser wavelength whilst having a bandwidth which is

not too broad, or useful scattered light will be lost. The characteristic produced by these filters in series is shown in Fig. 6. The overall rejection ratio is not as high as it would be if the filters were illuminated with near parallel light at normal incidence, due to the fact that input rays have a range of angles ($\pm$ 2.4°) about the mean angle of incidence of 15°. This means that not all the rays, for light with ruby laser wavelength, 'see' the maximum of the transmission characteristic. However, the present design has the virtue of simplicity and the absence of losses due to additional components necessary to produce near parallel light at normal incidence. In practice the rejection ratio obtained ($\sim$ 78:1) is sufficient to reduce stray laser light to a very low or negligible level, except for the channel adjacent to the laser line.

The intense burst of plasma light arising during the initiation phase of the plasma is prevented from reaching, and probably saturating, the photomultipliers by an electronically controlled optical shutter which opens completely in 4 ms, and can be set to remain open for a wide range of times so that all of the laser pulses can be accepted.

Immediately before the polychromator slit is a polarizing prism of the Glan-Thomson type, which transmits a very high fraction of the scattered light but rejects one half of the plasma light and thereby enhances the S/N ratio.

A yellow glass filter, which has a cut-off edge at a slightly lower wavelength than the shortest wavelength channel of the polychromator, is also included in the optics train. This filter prevents plasma radiation in the blue-green region of the visible spectrum, in particular impurity line radiation, from entering the polychromator where it could be diffracted twice from the grating and so cause a general defocused level of illumination over all of the fibre optic channels.

All surfaces within the system were anti-reflection coated for maximum transmission.

The system was designed to have unit magnification and the results from the ray tracing programme and the experimental value agree well with this figure.

Polychromator

The polychromator used is a slightly modified f/6 Rank Monospek 600. The grating equation describing the action of the grating is:

$$m\lambda = a(\sin\alpha + \sin\beta) \qquad \ldots (14)$$

where λ = wavelength of the light ($\mathring{A}$), a = groove spacing ($\mathring{A}$), α and β are the angles of incidence and diffration respectively (with appropriate signs), and m = the order of diffraction, which is arranged to be 1 in this case. Equation (14) can be rearranged to give:

$$\lambda = 2a \sin\left(\frac{\alpha + \beta}{2}\right) \cos\left(\frac{\alpha - \beta}{2}\right). \qquad \ldots (15)$$

But $\beta - \alpha = 2\phi \approx 22^{o}$, where 2ϕ is a fixed angle uniquely determined by the geometry of the Monospek. Solving for α we find:

$$\alpha = \psi - \phi \qquad \ldots (16)$$

where ψ = arc sin $(\lambda/2a \cos\phi)$. $\qquad \ldots (17)$

Also from the geometry of the Monospek, we deduce that the desired blaze angle is given by ψ.

The linear dispersion will be given by:

$$\frac{d\lambda}{dx} = \frac{a \cos\beta}{f\,m} \quad \mathring{A}\ mm^{-1} \qquad \ldots (18)$$

where f is the focal length of the Monospek (600 mm). The grating chosen to cover most of the temperature range of interest on DITE was manufactured by Jobin-Yvon, type No 23SM211R. This grating has 600 grooves mm^{-1}, and a ruled area measuring 110 mm × 110 mm. If we

take a typical wavelength within the scattered spectrum as $\lambda = 6500$ Å, then, by equations (16) and (17)

$$\alpha = 0.45^{o}.$$

This means that the grating is almost exactly at right angles to the collimated input beam, produced by the first mirror and therefore intercepts all the light passed through the entrance slit.

From equation (17), the value required for the blaze angle is 11.45^{o} and this is sufficiently close to that of the grating chosen (13^{o}) to ensure that the system works near peak efficiency. The scattered radiation is polarized in the horizontal plane, whilst the grooves of the grating are vertical. This also means that the grating will work at maximum efficiency.

Equation (18) yields a value for the dispersion of 25.7 Å mm^{-1} and this compares favourably with a measured value of 25.4 Å mm^{-1}.

As indicated earlier, the laser was found to be capable of focusing 90% of the energy over four pulses through a 2.5 mm diameter aperture and therefore the diameter of the scattering volume was chosen as 2.5 mm. Since the collection optics system has unit magnification the slit width of the polychromator was also set to 2.5 mm. Its height was fixed at 10 mm. In the Monospek the focal lengths of the collimating and focusing mirrors are equal with the result that the dimensions of the image of the input slit on the output plane will also be 2.5 mm × 10 mm.

The 10 equal fibre optic output channels were arranged to be symmetric within the output aperture of the polychromator. Each channel had a width of 2.5 mm whilst the height was 12 mm, thus obviating the necessity for precise alignment in the vertical direction. The transmission of each channel was measured in the laboratory. The best and worst figures were 54% and 48% respectively.

An OB10 glass prism, with one face at the Brewster angle for the laser radiation, was fixed adjacent to the last fibre optic channel at the long wavelength end of the spectrum. The wavelength setting of the polychromator was then adjusted so that any stray laser light would fall on the Brewster angled face, where most of it would be absorbed. This arrangement means that the central wavelength of the first fibre optic channel will be:

$$\lambda_1 = 6943 - 2.5 \times 25.4 = 6880 \text{ Å}$$

and the central wavelength of each subsequent channel will decrease by 63.5 Å.

A fast LED circuit is fixed adjacent to the focussing mirror. Short duration (20 - 30 ns) pulses of light from this source illuminate each of the fibre optic input channels. The unit can be used to check that the gain of an individual channel has not changed significantly.

H_α Radiation

Over a wide range of conditions the plasma will be an intense source of H_α (λ = 6563 Å) light. This radiation will illuminate channel 6 (λ = 6562 Å) of the polychromator so that the plasma signal will in general be very large for this channel. For this reason the signals from channel 6 are not included in the analysis routine. However, it has been noted on several occasions that the scattered signal can exceed the level of the H_α signal. The H_α light does not significantly affect the scattered signals in channels 5 and 7.

Detection System

The photon flux from each fibre optic channel is monitored by a photomultiplier, type EMI 9658RA. In this particular tube the photocathode is deposited on a multiple prism surface which causes multiple reflections of the incident light and so enhances the effective quantum efficiency of the photocathode. Typically, the tubes have a quantum efficiency of

7 → 7.5% at 7000 Å, rising to 10.5 → 11% at 6300 Å. A gain of ~ 10^6 can be easily achieved by these tubes.

The dynode chain used is shown in Fig. 7. The row of relatively low value capacitors are situated as close as possible to the photomultiplier base to minimise inductive loops and these provide the current for the four fast pulses.

The row of relatively large value capacitors (electrolytics) prevents changes in the dynode voltages greater than 1% when the quasi-steady current flows due to the plasma radiation. This steady current may last for ~ 0.2 s. These capacitors are for convenience situated some distance from the photomultiplier base since a fast response from their circuits is not required.

Figure 8 is a section through a photomultiplier housing showing the arrangement for locating and coupling the fibre optic lead to the photomultiplier. Details of the magnetic screening are also shown. At the output end, each fibre optic bundle has a diameter of 6.2 mm and is contained within an aluminium ferrule. The photomultiplier, perspex rod and fibre optic end are kept in contact by spring loading the base of the photomultiplier. High transmission at the photomultiplier/perspex and perspex/fibre optic interfaces is maintained by using an appropriate grease. The perspex rod is used to distribute the mechanical load on the photomultiplier window and also to expand the output beam from the fibre optic lead to a diameter of ~ 20 mm. This means that the calibration of the system is less likely to be affected by small movements, since the quantum efficiency can vary quite rapidly across the photocathode. The highly compressed 'O' ring holds the ferrule in position and also makes the joint completely light tight.

Although the photomultipliers are purposely situated at the end of the trolley remote from the machine they will nevertheless be subjected to the quasi-steady, stray magnetic fields associated with the various coil structures of the machine. In designing the magnetic screening of the photomultiplier housings the overall value of these stray fields was assumed to be 100 gauss, although in practice it will almost certainly be smaller. The outer shielding was made from "Hellefors Remko" iron, with an inside diameter of 62.4 mm and a thickness of 6.9 mm. Within this iron cylinder is a Mumetal cylinder with an inside diameter of 58 mm and a thickness of 1.6 mm. The end plate of the housing is also made of iron with a thickness of 7 mm. Simple theory indicates that the screening ratio for this combination should be at least 2600 with the result that the field within the Mumetal shield will be ~ 0.04 gauss, and at this level will have no material effect on the performance of the photomultiplier[15].

All of the photomultiplier housings are contained within an aluminium plate box which is insulated from the trolley assembly. This box is connected directly to a screened room by a copper pipe, within which the leads from the photomultipliers are located. In this way the photomultipliers are screened from electrical interference.

Data Acquisition and Processing

A schematic diagram of the data acquisition system is shown in Fig. 9. A Camac system absorbs signals from the photomultipliers, then subsequently interacts with a MOD 1 computer, which in turn interacts with the laboratory central computer (ICL 470) and a number of peripherals.

The intelligent part of the Camac system is the 7025 Programmable Dataway Controller, backed-up by a 110 A Hytec Store. The 7025 is capable

of a number of operations, including simple arithmetic. Up to 256 instructions can be specified for the 7025 and these are obtained from the 110A Store. The latter can hold up to a combined total of 256 instructions and/or experimental data. Three Read-only-Memories are also contained in the 110A. These enable a program, on a paper tape, to be read into the memory from a teletype (TTY); the entire contents of the memory reproduced on a paper tape and, in addition, an editor facility can be used to change or read the contents of any memory location.

Signals from the ten photomultipliers and the fast diode monitor are integrated and digitised by two Nuclear Enterprises 9040/A Octal ADC's. Each of these units has 8 channels but they are programmed to look like one unit with 12 channels. These units have a nominal sensitivity of 0.4 pC/count and a full scale input of 100 pC. Gates for the 9040, at the appropriate times, are provided by a Gate Pulse Generator Type 8293-1, developed at Culham Laboratory. The 8293 is itself triggered from a signal generated by a fast vacuum diode which samples a very small fraction of the laser beam immediately outside the amplifier head. There is a delay of $\sim$ 100 ns between the arrival of the fast diode signal in the scattering screened room and the photomultiplier signals due to the total optical path of $\sim$ 10 m, the transit time of the electron bunch along the dynode chain ($\sim$ 55 ns) and the slightly slower cables used in the photomultiplier circuits. The gate width is set to $\sim$ 100 ns in order to straddle all of the photomultplier signals. The latter arrive at slightly different times due to the different transit times along the dynode structures. Each transit time is in turn a function of the voltage applied to the relevant photomultiplier.

One of the 7061 units enables information to be received from/sent to a TTY. The TTY displays nett signal and background levels for each channel after a DITE pulse; enables a 'Stand Alone' program to be

loaded in the 110A, when the MOD 1 is not available, and also facilitates programme editing. The other 7061 unit enables the Camac system to interact with the MOD 1 via an optical link; the latter being included to prevent electrical interference reaching the equipment in the screened room. The Control Panel enables comprehensive checks to be made on the software in the 7025.

A typical sequence of events during a DITE pulse is as follows:

1. A few seconds before a DITE machine shot the programme in the 110A is refreshed with a copy of the same programme stored on the disc associated with the MOD 1. The machine shot number is also transferred to the 110A at this time and the position of the trolley is monitored.
2. The gate generator is then triggered by the pulse from the fast diode when the laser operates.
3. After a suitable delay, adjustable at the generator, both of the 9040 units are gated so as to integrate the photomultiplier signals.
4. The signals in the 12 9040 channels are then digitised and transferred sequentially to the 110A store. This process takes approximately 200 μs.
5. The two 9040's are then automatically gated again by the generator for a duration identical with the first gate. In this way the plasma light level in each channel is monitored. The signals are again passed to the 110A store.
6. The above process is repeated for the subsequent laser pulses, with a minimum time between laser pulses of about 400 μs.
7. A few seconds after the machine pulse all of the raw data is passed to the MOD 1, for detailed analysis, and is also output to the TTY in a partially processed form. This record can be examined immediately to check that all channels and the system as a whole are working correctly and that signal levels are reasonable.

8. When the 470 computer has completed the full analysis of the raw data, the results are returned to the MOD 1 which displays them on a VDU in the DITE area. Graphs of temperature and density versus minor radius can also be obtained when required.

The stray laser light level in all channels can be easily checked by operating the complete system between DITE machine pulses, i.e. when no plasma is present in the torus.

Although not described above, the gating generator can be set to operate in a different mode in association with the 9040's so that scattering signals could be recorded when the delay between laser pulses is much less than the 400 μs mentioned above. However, as yet the system has not been used in this mode.

SYSTEM CALIBRATION

Three separate aspects of the calibration of the optical, detection and data acquisition systems can be identified:

a) The relative response of channels to given luminous power input needs to be known as accurately as possible since this relative calibration, when applied to the raw data, largely determines the value of the temperature.

b) The absolute value of the gain for each photomultiplier needs to be deduced so that the number of photoelectrons giving rise to each signal can be estimated. The errors on each signal depend directly on the number of photoelectrons and these errors influence the final results through the weighting function used in the computer fitting routine.

c) The absolute calibration of the channels will enable a global constant to be calculated for the system so that the plasma density can be deduced directly from the density figure produced by the computer fitting routine.

The most direct way of obtaining an absolute calibration of the system is by the technique of Rayleigh scattering from a gas within the DITE torus. However, Rayleigh scattering is inappropriate in this instance due to the presence of the two notch filters. By necessity, the calibrations are therefore performed using standard lamps and ancilliary apparatus at wavelengths other than 6943 Å, but, because these measurements are made with the scattering trolley in its most remote position with respect to the torus, the viewing window is not included in the region between the scattering volume and the objective lens. This means that possible loss of transmission at the viewing window due to an evaporated metallic film, caused by plasma-wall interactions, is not taken into account. It should be pointed out that when one of these metallic films was examined the absorption, over the wavelength band of interest in this experiment, was found to vary by only a few per cent, with the result that the effect on a typical temperature would be relatively small.

Two different standard lamp arrangements have been used and these are illustrated in Fig. 10. The first technique employed a radiance standard (Ribbon filament calibrated in power at a given wavelength per unit solid angle per unit wavelength interval) with its filament at the position of the scattering volume and one or more high grade calibrated neutral density filters between the filament and the objective lens. A possible weakness in this technique is that even a microscopic hole in the filter could cause a large error because the transmission ($\sim 10^{-5} - 10^{-4}$) of these filters is extremely low. Inaccuracies can also arise due to multiple reflections when the filters are used.
In the second method an irradiance standard (power at a given wavelength per unit wavelength interval per unit area at a given distance from the filament) was used in conjunction with a plaque of Russian opal glass, type MS20. In this technique no form of attenuation was required either

between the filament and plaque or between the plaque and objective lens. Calibration tables were supplied by N.P.L., Teddington for both of the lamps and the opal glass plaque.

In the calibration measurements the D.C. current from each photomultiplier was measured using an accurate microammeter. The sensitivity of the 9040 gated integrator was checked separately.

Standard Lamp Measurements

For the case of the radiance standard the output of each channel takes the form:

$$I_a = eT_s G\eta \Omega A_F W \frac{n_R}{\delta} \quad \ldots (19)$$

where I_a = Current output of the photomultiplier

T_s = Transmission of the system

G = Electrical gain of the photomultiplier

η = Quantum efficiency of the photocathode

A_F = Relevant area of filament from which radiation is collected.

n_R = Photons s^{-1} $\mathring{A}^{-1}$ $Ster^{-1}$ mm^{-2} leaving A_F at the appropriate wavelength in the horizontal plane of polarization only.

δ = Attenuation ratio across neutral density filter(s) $(10^4 - 10^5)$.

Ω, W = previously defined.

For the irradiance standard:

$$I_a' = eT_s G \eta \Omega A_s n_I \quad \ldots (20)$$

where A_s = area of polychromator slit imaged on plaque

n_I = photons s^{-1} mm^{-2} $Ster^{-1}$ $\mathring{A}^{-1}$ from surface of plaque in the horizontal plane of polarization only.

The other parameters are as above.

Relative Gain Adjustments

The sensitivity of each channel was adjusted, by varying the gain of each photomultiplier, so that every channel would produce the same current output for the same luminous power input. In practice this meant that all channels were set relative to channel 10, with the ratio of the current in channel 10 to the current in any other channel being equal to the ratio of the lamp power for channel 10 to the lamp power for the other channel. This procedure was repeated with both types of lamp. The relative intensity calibrations were found to differ by only 4.4% when the system was initially calibrated with one lamp arrangement and subsequently checked with the other.

Estimates for the Absolute Gains

The value of G for channel 10 was measured in the laboratory as accurately as possible with a standard lamp arrangement. From equations (19) and (20) we can see that G can be determined for all of the other channels, if values of η and T_s are available, by comparing the current flowing in the other channels with that in channel 10. Values of η versus wavelength were not available for each photomultiplier and were therefore estimated from a combination of point measurements at 7000 Å for all the photomultipliers and extrapolations from these points along curves which were parallel to a set of curves of η versus wavelength available for a group of photomultipliers manufactured shortly after the batch used in this experiment. The value of T_s was assumed to be constant for all the channels, although this assumption has not been checked by measurement on the complete system. One of the most likely causes of variation in T_s is due to differences in the transmission of the fibre optic channels. However, as indicated earlier the transmission was found to be constant to within $\sim$ 12%. Thus, with the assumption that T_s was constant the value of G was derived for all the other channels by noting the value of I_a and calculating the appropriate value for n_R. The values

for G can then be used in equation (12) to obtain for each channel the ratio:

$$g = \frac{C}{n_{pe}} = \frac{eG}{S} \text{ counts/photoelectron} \quad \ldots (21)$$

and this ratio is used in the computer routine for the calculation of the errors on each signal. It should be emphasised that these estimates for the absolute values of G do not influence the actual magnitude of the signals; this latter property is set in the relative gain adjustments of the channels. The values derived for η, G and g for each channel are summarised in Table II.

Absolute Calibration for the Electron Density

The implication of the relative calibration is that:

$$\frac{I_a}{I_L} = \text{constant}$$

where I_L is the lamp power at the relevant wavelength.

But $$I_L = \frac{h\,c\,n_R}{\lambda_s}$$

where h and c are fundamental constants

n_R = photon rate from lamp

λ_s = central wavelength of channel

$$\therefore \quad \frac{I_a \lambda_s}{n_R} = \text{constant, for all channels.} \quad \ldots (22)$$

Equation (19) can be rearranged to yield:

$$G\,\eta\,T_s = \frac{I_a}{n_R}\left(\frac{\delta}{e\Omega\,A_F\,W}\right)$$

and we can multiply each side by λ_s to obtain:

$$G\,\eta\,T_s\,\lambda_s = \frac{I_a \lambda_s}{n_R}\left(\frac{\delta}{e\Omega\,A_F\,W}\right). \quad \ldots (23)$$

Using equation (22) and the fact that all the parameters within the brackets are constants we deduce:

$$G \eta T_s \lambda_s = \text{constant, for all channels.} \quad \ldots (24)$$

We are now in a position to derive the global constant which relates the density figure produced by the computer routine to the actual electron density at the scattering volume.

The signal (in counts) due to scattered radiation for any channel is given by:

$$C = n_p T_s \eta G e/S \quad \ldots (25)$$

where n_p is given by a slightly modified version of equation (4):

$$n_p = k n_e \lambda_s T_e^{-\frac{1}{2}} f \exp(\varepsilon/T_e) \quad \ldots (26)$$

where $k = 3.32 \times 10^{-31} N_L L \Omega W$ and $N_L = 3.5 \times 10^{18} D/r$

r = diode sensitivity in counts/joule

D = diode signal in counts

$\varepsilon = -\alpha \Delta\lambda^2 (1 - \Delta\lambda/\lambda_L)$ and $\Delta\lambda = \lambda_s - \lambda_L$

α = constant

$$\therefore \quad C = k n_e \lambda_s T_e^{-\frac{1}{2}} T_s \eta G \frac{e}{S} f \exp(\varepsilon/T_e).$$

For mathematical convenience each side of this equation is multiplied by the term

$$\omega f \exp(\varepsilon/T_e)$$

(where ω is the weighting function associated with the given channel) in order to convert this equation into a form similar to the one derived for the computer fitting routine (see Appendix) which produces the density figure. Thus we have:

$$C \omega f \exp(\varepsilon/T_e) = k n_e T_e^{-\frac{1}{2}} T_s \eta G \lambda_s \frac{e}{S} \omega f^2 \exp(2\varepsilon/T_e).$$

The equation can now be summed over all channels used in the analysis routine to give:

$$\Sigma C \omega f \exp(\varepsilon/T_e) = \frac{ek n_e T_e^{-\frac{1}{2}}}{S} \Sigma T_s \eta G \lambda_s \omega f^2 \exp(2\varepsilon/T_e).$$

But from equation (24) $T_s \eta G \lambda_s$ = constant

$$\therefore n_e = \left(\frac{\Sigma_2}{\Sigma_3}\right) \frac{S T_e^{\frac{1}{2}}}{ek T_s \eta G \lambda_s} \quad \ldots (27)$$

where $\Sigma_2 = \Sigma C \omega f \exp(\varepsilon/T_e)$

$\Sigma_3 = \Sigma \omega f^2 \exp(2\varepsilon/T_e)$.

The figure produced by the computer routine for the electron density is given by

$$n_e' = 0.01 D^{-1} T_e^{\frac{1}{2}} \alpha^{-\frac{1}{2}} \Sigma_2/\Sigma_3 \quad \ldots (28)$$

where $\alpha = 2.65 \times 10^{-3}$. Thus the expressions (27) and (28) can be equated providing equation (28) is multiplied by the global constant, say C_n. We obtain:

$$C_n = \frac{5.15 S D}{ek T_s \eta G \lambda_s} . \quad \ldots (29)$$

Using the previous definition of k, the value of $T_s \eta G \lambda_s$ from equation (23), the fact that only ~ 0.9 of the laser energy traverses the scattering volume and that T_s needs to be multiplied by 0.93 because the viewing window is not in the system when the lamps are used, then we finally derive:

$$C_n = 5.34 \times 10^{13} \left(\frac{r I_L A_F}{L I_a \delta} \right). \quad \ldots (30)$$

A similar expression can be derived for the case of the irradiance lamp, and takes the form:

$$C_n' = 1.7 \times 10^{10} \left(\frac{A_s r I_L' \beta}{L I_a'} \right). \quad \ldots (31)$$

It should be noted that the above values for the global constant do not depend on knowing any of the particular performance parameters of the photomultipliers or the transmission of the system.

DATA ANALYSIS

The data analysis routine used in this experiment follows closely a technique developed by W. Millar of Culham Laboratory. This routine is described in some detail in the Appendix of this report.

RESULTS

Radial profiles obtained with the scattering apparatus, for different DITE plasmas, have been published elsewhere[9,17,18,19,20]. The results discussed here therefore deal with data from individual pulses, and with comparisons of results obtained by the scattering apparatus and other diagnostics.

Intensity Versus Wavelength Plots

Most of the individual results from the apparatus have been obtained in the form of intensity versus wavelength plots from the computer. An example is shown in Fig. 11, which had two laser pulses during one machine pulse. The number of channels used in the fitting routine is usually 8, the innermost channel being neglected due to stray light and the 6th channel due to the presence of H_α light.

The data line above each plot presents the temperature, standard deviation of the temperature, machine shot number and the time, in ms after the start of the plasma current, when the laser was pulsed. Shown within the frame are the radial position of the scattering volume in cm and the reduced value of chi-squared for that plot. Beneath the frame is a figure proportional to the electron density and its standard deviation. Values for T_e, σ_T, n_e and σ_n are calculated from equations (38), (40), (28) and (42) respectively, as indicated in the Appendix. The value of CHISQN is found by dividing the minimum result from equation (32) by the number of degrees of freedom (6 in this case).

From the plots there is no visual evidence for a non-Maxwellian distribution of electron energies, with the outermost channel sampling electron energies (perpendicular to the main toroidal field) up to $\sim$ 2 keV.

Analysis of Chi-squared Data

The technique used for analysing a batch of reduced chi-squared data is described in the Appendix to this report. Results from this analysis give an overall indication of how well theory and experiment agree.

So far 90 values of the reduced chi-squared parameter have been obtained from runs of the fitting routine. In all of these runs the number of channels used in the fitting routine has been 8 with the result that the number of degrees of freedom, ν, has been 6.

The frequency distribution of the observed reduced chi-squared data is shown as a histogram in Fig. 12. Five observed values lie to the right of x = 2.5 and do not therefore appear on the figure. Also shown in the figure (as a continuous curve) is the expected frequency distribution given by equation (50) with N = 90, Δ = 0.1, ν = 6 and with x taking the values 0.05, 0.15, ... 2.45. The peak of the expected frequency distribution curve occurs at x = 0.67, as given by equation (49).

Applying equation (51) to the results shown in Fig. 12 we find that χ_o^2 = 27.2. The relevant number of degrees of freedom (number of intervals in the histogram less one) is 24 and therefore from statistical tables the probability of the above value of χ_o^2 being exceeded is $\sim$ 0.3. At this level the probability indicates reasonable overall agreement between theory and experiment and is therefore encouraging, but clearly many more data are needed before any firm conclusions can be drawn.

X-Ray Temperatures

The laser scattering results for the central electron temperature are compared with those measured with the X-ray spectrometer in Fig. 13. It can be seen that there is good agreement between the two methods. The X-ray results[21] are obtained by line-of-sight measurements through the plasma with a system (similar to that constructed elsewhere[22]) employing a Si(Li) cooled detector and pulse height analysis. These experimental results are then compared with a computer model of the plasma emission. By the nature of the experiment the results are heavily weighted on the conditions existing in the central region of the plasma. It should be noted that the X-ray data are obtained by integrating signals over many milliseconds during a discharge so that

the derived temperature is a temporal average. If more than one laser temperature was available during the integrating period then those too were averaged.

Electron Cyclotron Emission Profile

A radial profile of electron temperature from the E.C.E. diagnostic[23] and results from the scattering system are compared in Fig. 14. The level of agreement is seen to be good. The E.C.E. profile[24] is normalised to the scattering results by setting the ordinate of the right hand peak equal to the scattering result for a minor radius of + 5 cm. From the figure it can be seen that the level of agreement between the two techniques could be improved if the entire E.C.E. profile were shifted (~ 1.7 cm) so that the central dip coincided with zero minor radius. However, the size of this discrepancy is probably within the total spatial accuracy of the two diagnostics. It should be noted that the E.C.E. profile was measured in one machine pulse whilst the scattering results were obtained from several shots and therefore include any shot-to-shot irreproducibility.

Electron Density Profile

A comparison of the density profile obtained with the laser system and the mircowave interferometer is shown in Fig. 15. The solid line shows the profile from the 2 mm microwave interferometer[25] which is obtained by Abel inversion of line-of-sight measurements using several channels. The uncorrected laser data were all multiplied by the constant 0.62×10^{13} in order to bring the two sets of results into coincidence. This constant can be compared with the global constant derived from the standard lamp measurements. The results from the irradiance lamp are preferred in this case because no large attenuation factor ($\sim 10^5$) is required in this system. In equation (31) we have $A_s = 25\ mm^2$, $I_L' = 4.02\ mW\ m^{-2}$, $L = 1$ cm, $I_a' = 12.7\ \mu A$, $\beta = 1$ to a good approximation for the conditions under which the plaque is used, and for this set of

measurements r = 50 counts/Joule.

Hence $C_n' = 0.67 \times 10^{13}$.

The level of agreement is almost certainly fortuitous but it nevertheless demonstrates that the laser and microwave results are in substantial agreement.

CONCLUSIONS

A multi-pulse ruby laser scattering system has been designed and constructed which has worked successfully and produced several thousand results. It has run for periods of several months without requiring any form of realignment.

Good agreement is found when results are compared with those obtained from other diagnostics.

ACKNOWLEDGEMENTS

The author wishes to thank Dr J.W.M. Paul for his help and encouragement in this work, colleagues for use of their results, Dr J. Hugill who was responsible for the IDA data processing program, which includes the fitting routine for the scattering experiment as one section, and Mr M. Dunstan for his invaluable assistance with this project.

APPENDIX

DATA ANALYSIS

Fitting Routine

The basis of the analysis routine is to find the minimum of the sum defined by:

$$\Sigma_1 \equiv \chi^2 \equiv \Sigma\, \omega \{y - \zeta\,(T_e,n)\}^2 \qquad \ldots (32)$$

where y = nett observed signal

$\zeta(T_e,n)$ = theoretical signal

ω = statistical weighting function

n = proportional to electron density

and Σ is over all of the channels used in the analysis.

The expression for $\zeta(T_e,n)$ is equivalent to that given by equation (4) for P_{sc} but is written in the more convenient form:

$$\zeta = T_e^{-\frac{1}{2}}\, \alpha^{\frac{1}{2}}\, n\, f\, \exp(\varepsilon/T_e). \qquad \ldots (33)$$

For Σ_1 to be a minimum we need:

$$\frac{\partial \Sigma_1}{\partial n} = 0 \qquad \ldots (34)$$

and

$$\frac{\partial \Sigma_1}{\partial T_e} = 0 \qquad \ldots (35)$$

Equation (34) yields $n = T_e^{\frac{1}{2}}\, \alpha^{-\frac{1}{2}}\, \Sigma_2/\Sigma_3$ ... (36)

where $\Sigma_2 = \Sigma\, \omega\, y\, f\, \exp(\varepsilon/T_e)$

and $\Sigma_3 = \Sigma\, \omega\, f^2\, \exp(2\varepsilon/T_e)$.

It should be noted that equations (36) and (28) are identical, except for the correction to (28) due to the diode signal.

Using the expression from equation (36) in equation (32) yields:

$$\Sigma_1 = \Sigma_4 - \Sigma_2^2/\Sigma_3 \qquad \ldots (37)$$

where $\Sigma_4 = \Sigma\ \omega\ y^2$.

Differentiation of equation (37) with respect to T_e gives

$$\frac{\partial \Sigma_1}{\partial T_e} = 0 \quad \text{when}$$

$$G \equiv \Sigma_3\ \Sigma_5 - \Sigma_2\ \Sigma_6 = 0 \qquad \ldots (38)$$

where $\Sigma_5 = \Sigma\ \omega\ y\ \varepsilon\ f\ \exp(\varepsilon/T_e)$

$\Sigma_6 = \Sigma\ \omega\ \varepsilon\ f^2\ \exp(2\varepsilon/T_e)$.

The computer program finds by means of an iteration technique a value for T_e which yields a solution for equation (38) (no proof is given that this solution is necessarily unique). This value of T_e, together with the value of n obtained from equation (36), yields a minimum value for χ^2.

For σ_T and σ_n, the errors on the temperature and density respectively, use is made of the small-error theorem[16], which states that for any parameter Q, with uncorrelated errors in its variables:

$$\sigma_Q^2 = \Sigma\ \omega^{-1} \left(\frac{\partial Q}{\partial y} \right)^2.$$

Thus for $Q = T_e$ we obtain:

$$\sigma_T^2 = \Sigma\ \omega^{-1} \left(\frac{\partial G}{\partial y} \right)^2 \Big/ \left(\frac{\partial G}{\partial T_e} \right)^2 \qquad \ldots (39)$$

Finally we obtain:

$$\sigma_T = T_e^{\,2}\ \Sigma_9^{\frac{1}{2}} / \Sigma_{10} \qquad \ldots (40)$$

where $\Sigma_7 = \Sigma\ \omega\ y\ \varepsilon^2\ f\ \exp\ (\varepsilon/T_e)$

$\Sigma_8 = \Sigma\ \omega\ \varepsilon^2\ f^2\ \exp\ (2\varepsilon/T_e)$

$\Sigma_9 = \Sigma_3\ (\Sigma_3\ \Sigma_8 - \Sigma_6^2)$

$\Sigma_{10} = \Sigma_3\ \Sigma_7 + \Sigma_5\ \Sigma_6 - 2\Sigma_2\ \Sigma_8$.

For Q = n, and using equation (36), we obtain:

$$\sigma_n^2 = \alpha^{-1} \Sigma \omega^{-1} \{\frac{\partial}{\partial y} (T_e^{\frac{1}{2}} \Sigma_2/\Sigma_3)\}^2$$

which yields:

$$\sigma_n^2 = \alpha^{-1} \Sigma_3^{-2} \{T_e \Sigma_3 + 0.25 T_e^{-1} \Sigma_2^2 \sigma_T^2\}. \quad \ldots (41)$$

Using equation (40) we finally obtain:

$$\sigma_n^2 = \alpha^{-1} (P_A + P_T) \quad \ldots (42)$$

where $P_A = T_e/\Sigma_3$

and $P_T = 0.25 \Sigma_3^{-2} \Sigma_{10}^{-2} \Sigma_2^2 \Sigma_9 T_e^3$.

We now need to derive an expression for the weighting function ω, which is individually calculated for each channel in the analysis routine. The assumption is made that the errors are normally distributed about the measured values. In fact, the errors on the photomultiplier signals are determined by Poisson statistics. However, except for signals derived from only a few photoelectrons, typically in the channels most remote from the laser wavelength, the Poisson distribution is a reasonable approximation of the normal distribution. By the principle of weighted least squares we have that:

$$\omega = \sigma_y^{-2} \quad \ldots (43)$$

where σ_y is the standard deviation associated with the nett signal y.

The value of y (in counts) for any channel is given by:

$$y = s - b - \frac{p}{\mu} \quad \ldots (44)$$

where s = signal counts (scattered signal + background)

b = background counts

p = <u>total</u> stray light counts obtained over μ stray light shots.

The number of photoelectrons, ϕ, corresponding to y is given by:

$$\phi = (s - b - \frac{p}{\mu})/g,$$

where g is given by equation (21).

Using the rules for the propagation of errors[16] and the fact that ϕ is distributed according to Poisson statistics, we obtain:

$$\sigma_{\phi}^2 = (s + b + \frac{p}{\mu^2})/g. \quad \ldots (45)$$

But

$$\sigma_y^2 = g^2 \sigma_{\phi}^2. \quad \ldots (46)$$

Using equation (46) in equation (45) we obtain:

$$\omega^{-1} = \sigma_y^2 = (s + b + \frac{p}{\mu^2})g. \quad \ldots (47)$$

The possibility of applying an infinite weight to a point, in the rare case when $s = b = p = 0$, is avoided by assigning a minimum value to σ_y^2 in the computer program. Digitisation errors are not considered in equation (47), but in general for reasonable signals their effect is very small.

χ^2 Analysis

In the above fitting routine the value of the fitting parameter χ^2 is calculated as a matter of course, each time values of temperature and density are produced although its value has not been an output from the computer with the other results until recently. An individual value of χ^2 associated with one temperature and density measurement will give an indication of the reliability of that measurement and, in addition, an examination of the distribution of values of χ^2 for a large number of pulses can yield useful statistical information on how well the experimental data fits the theoretical spectral distribution given by equation (4).

The probability distribution for the fitting parameter is given by[16]:

$$p(x,\nu) = \frac{1}{2^{\nu/2}\Gamma(\nu/2)} (x\nu)^{\nu/2-1} e^{-x\nu/2} \quad \ldots (48)$$

where $x = \chi^2/\nu$ is the reduced form of chi-squared and ν is the number of degrees of freedom in the system.

Simple analysis of equation (48) shows that the peak of the distribution occurs at

$$x = (\nu - 2)/\nu. \qquad \ldots (49)$$

If we have a total population of N values of reduced chi-squared and we divide the variable x into a number of equal intervals of width Δ, then, providing Δ is sufficiently small, the expected frequency, E(x), in the interval $x - \Delta/2 \rightarrow x + \Delta/2$ is given by:

$$E(x) = N \Delta \nu \, p(x,\nu). \qquad \ldots (50)$$

If the corresponding observed frequency in the same interval is O(x) then we can calculate an overall value of chi-squared, χ^2_o, given by:

$$\chi^2_o = \sum \frac{\{O(x) - E(x)\}^2}{E(x)} \qquad \ldots (51)$$

where the summation is calculated over a sufficiently large number of intervals in x to include all, or almost all, of the observed values of x.

The value of χ^2_o found from equation (51) can then be used in standard statistical tables to determine the probability of the N observed values of x being a truly random set distributed according to equation (48). An abnormally low value for this probability indicates a considerable disagreement between experiment and theory.

REFERENCES

(1) A.J. Bearden et al, Phys. Rev. Letts. 6, 257 (1961).

(2) A.N. Dellis, Third Int. Conf. on Ioniz. Phenom. in Gases, Venice, 228 (1957).

(3) L.A. Artsimovich, Nuclear Fusion, 12, 215 (1972).

(4) G.N. Harding et al, Proc. 2nd U.N. Int. Conf. on Peaceful Uses of Atomic Energy, Geneva, 32, 365 (1958).

(5) D.E. Evans and J. Katzenstein, Rep. Prog. Phys. 32, 207 (1969).

(6) A.W. De Silva and G.C. Goldenbaum "Methods of Experimental Physics" Vol, 9, Part A, p.61 Ed. H.R. Griem and R.H. Lovberg, Academic Press, New York (1970).

(7) J. Sheffield "Plasma Scattering of Electromagnetic Radiation", Academic Press, New York (1975).

(8) M.J. Forrest et al, UKAEA Report CLM-R107 (1970).

(9) J.W.M. Paul et al, Proc. 6th Int. Conf. on Plasma Physics and Controlled Fusion Research, Berchtesgaden (1976), I.A.E.A. Vienna, 2, 269 (1977).

(10) M. Mattioli and R. Papoular, Plasma Physics 17, 165 (1975).

(11) M.A. Heald and C.B. Wharton "Plasma Diagnostics with Microwaves", p.248 Wiley, New York (1965).

(12) W.J. Karzas and R. Latter, Astrophys. J. Supp. Series, 6, 167 (1961).

(13) N. Bretz et al, Report PPPL-1356 (1977).

(14) C.A. Steed and E.G. Murphy "On Line Computing in the Laboratory" p.333 Ed. Rosner et al. "International Tracts in Computer Studies", Advanced Publications Ltd (1976).

(15) E.M.I. Brochure. P001/fp70,p.8,(1970).

(16) P.R. Bevington "Data Reduction and Error Analysis" McGraw-Hill, New York (1969).

(17) S.J. Fielding et al, Nuc. Fus. Letts. 176, 1382 (1977).

(18) R.D. Gill et al, 8th European Conf. on Controlled Fusion and Plasma Phys. Prague, 1, 171 (1977) and Culham Preprint CLM-P492.

(19) J. Hugill et al, 1,39 ibid and Culham Preprint CLM-P 492.

(20) P.E. Stott et al, Symp. on Plasma-Wall Interactions, Julich (1976).

(21) R.D. Gill, Private Communication (1978).

(22) S. Von Goeler et al, Report MATT-1060 (1974).

(23) P. Brossier et al, Proc. 6th Int. Conf. on Plasma Physics and Controlled Fusion Research, Berchtesgaden (1976) and I.A.E.A. Vienna, I, 409 (1977).

(24) A.E. Costley, Private Communication (1978).

(25) J. Hugill, Private Communication (1978).

TABLE I

	Channel 1	Channel 10
Scattered Photons	50,400	2,900
Plasma Photons	11,200	12,200
Photoelectrons due to Scattered Photons	378	30
Photoelectrons due to Plasma Photons	84	128
S/N	41:1	2.7:1
A.D.C. Counts	151	12

TABLE II

Channel	λ_s Å	η (%)	Lamp Rel. Ratio	I (μA)	G ($\times 10^{-6}$)	g Counts/p.e.
1	6880	2.0	1.34	0.68	0.62	4.0
2	6816	8.0	1.30	6.61	1.57	1.59
3	6752	8.2	1.26	6.43	1.55	1.61
4	6689	8.6	1.22	6.24	1.49	1.68
5	6625	9.0	1.19	6.04	1.43	1.75
6	6562	9.5	1.15	5.85	1.37	1.82
7	6498	10.2	1.11	5.7	1.30	1.92
8	6435	10.5	1.07	5.5	1.27	1.97
9	6371	13.0	1.04	5.3	1.04	2.4
10	6308	11.4	1	5.1	1.19	2.1

Electron temperature scattering apparatus.

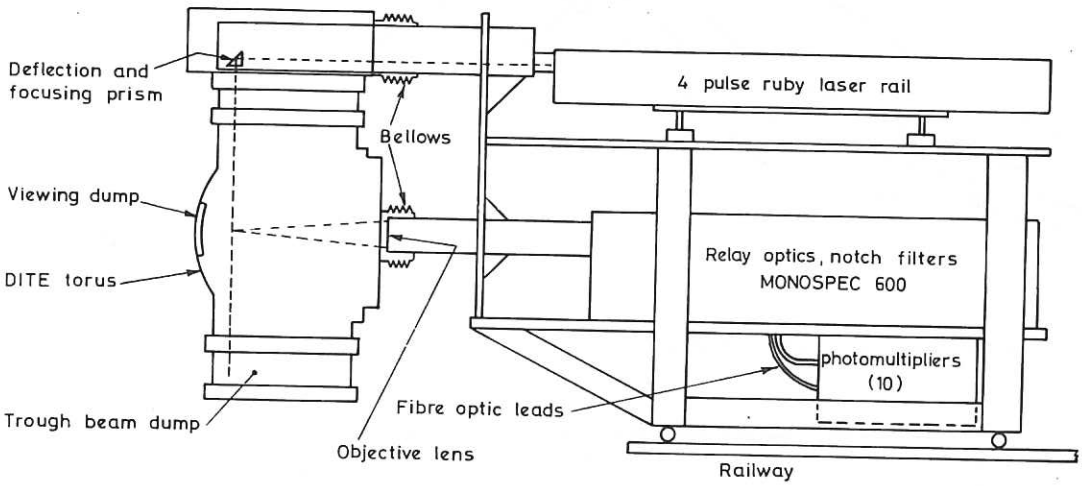

Fig. 1 Trolley assembly

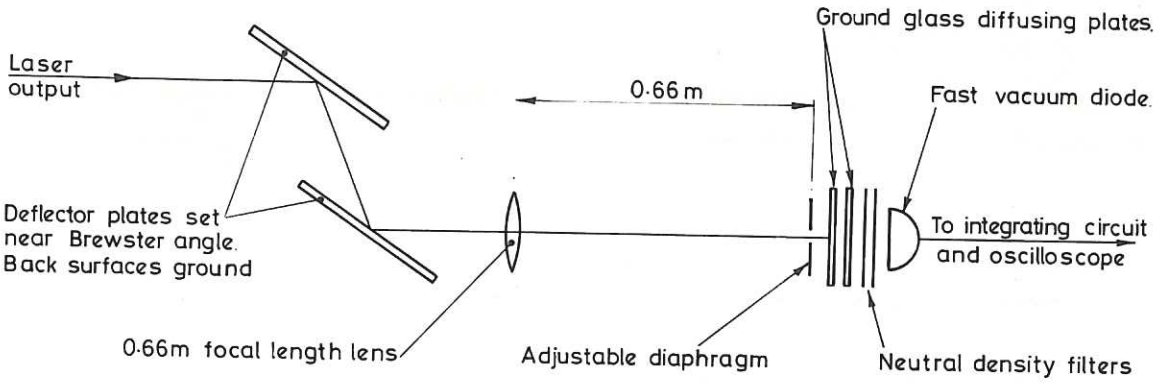

Fig. 2 Schematic of apparatus for beam divergence measurements.

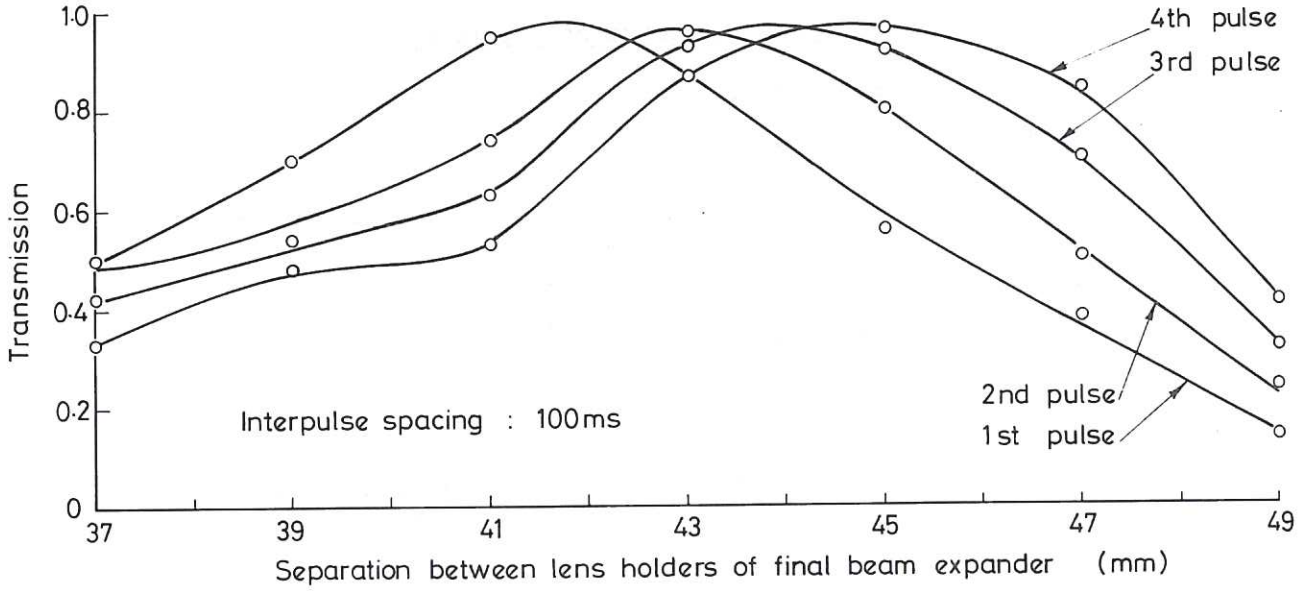

Fig. 3 Fraction of energy in each pulse passing through 2·5mm aperture.

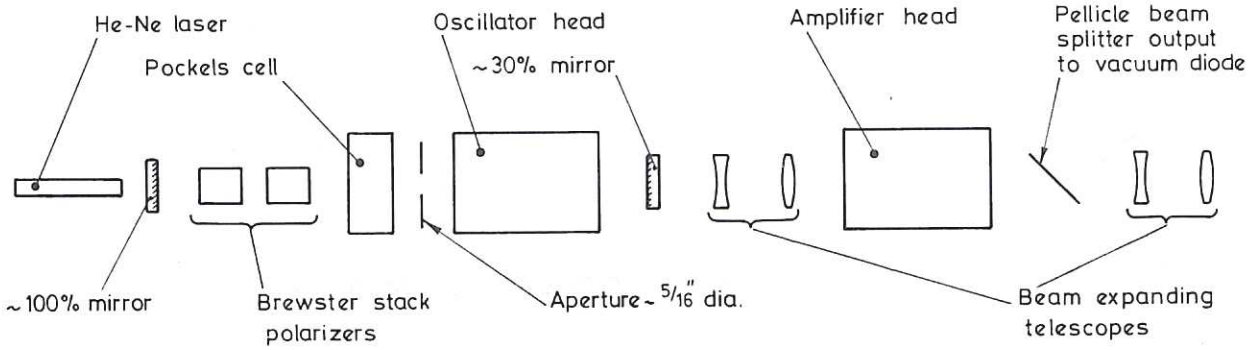

Fig. 4 Arrangement of components on laser bench

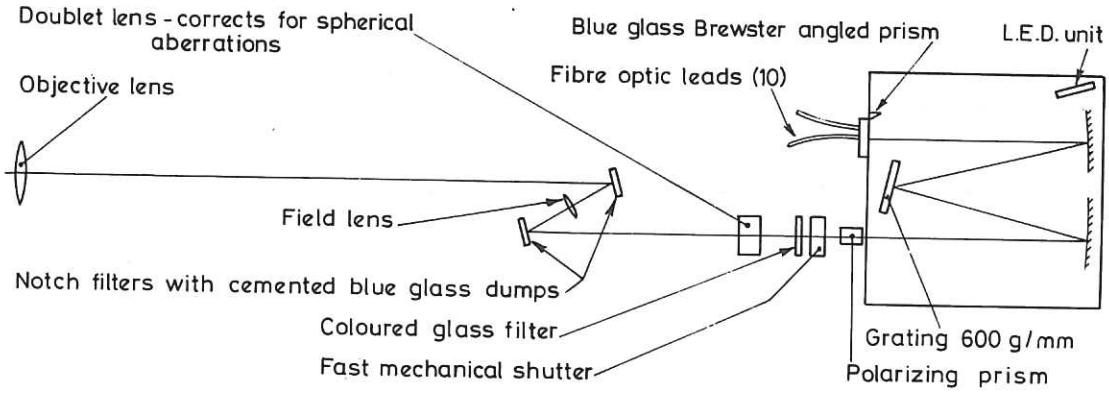

Fig. 5 Optical arrangement

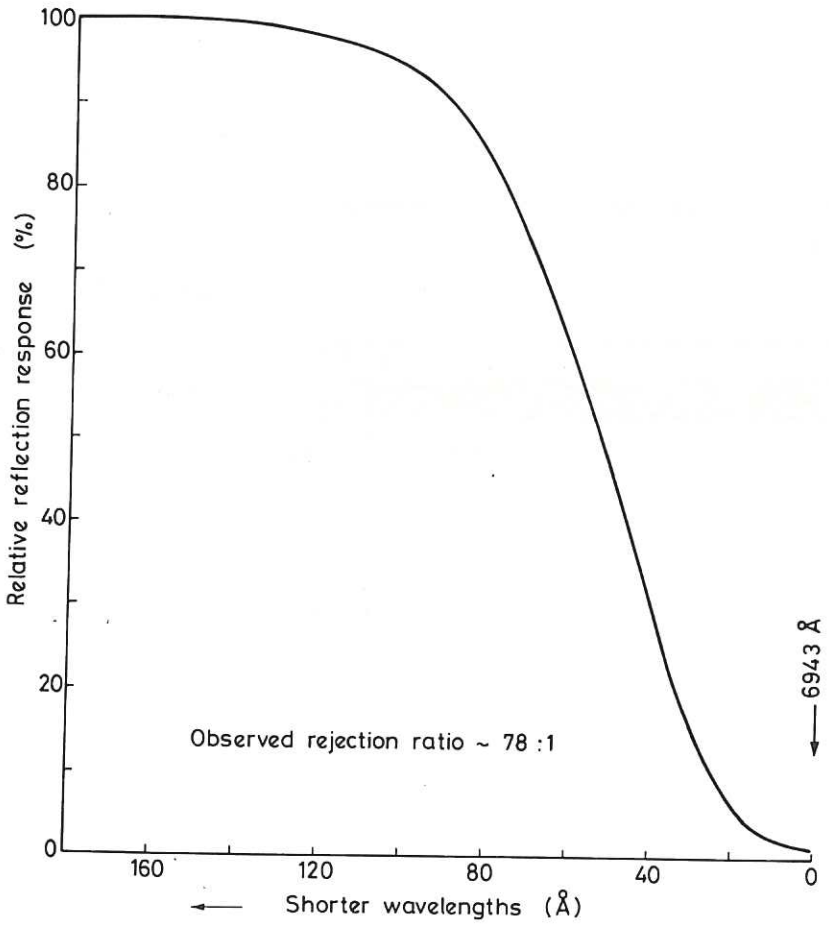

Fig. 6 Characteristic for the two notch filters in series.

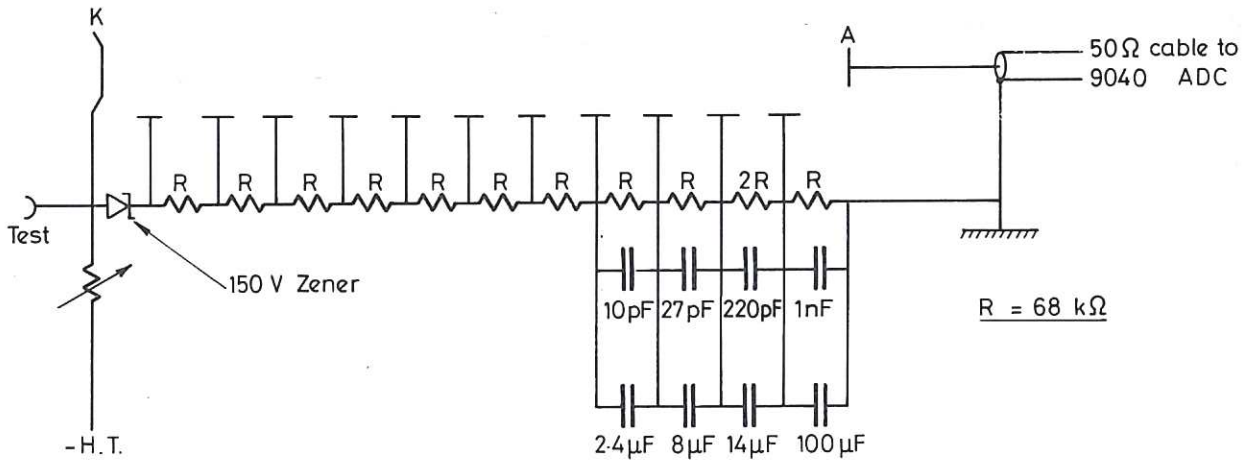

Fig. 7 Schematic of photomultiplier dynode chain

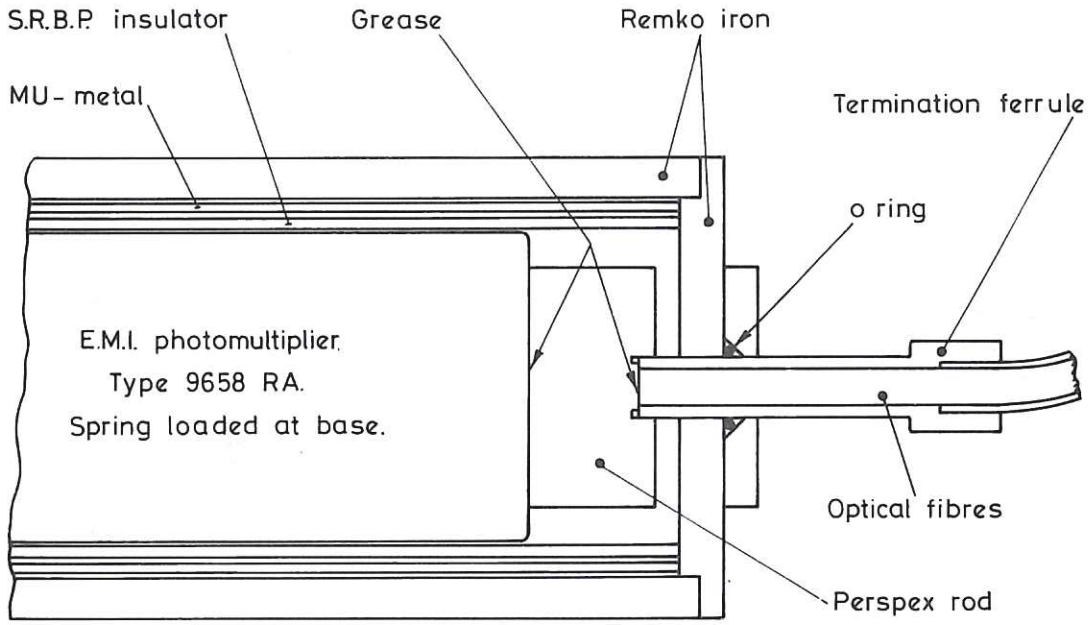

Fig. 8 Section through photomultiplier housing

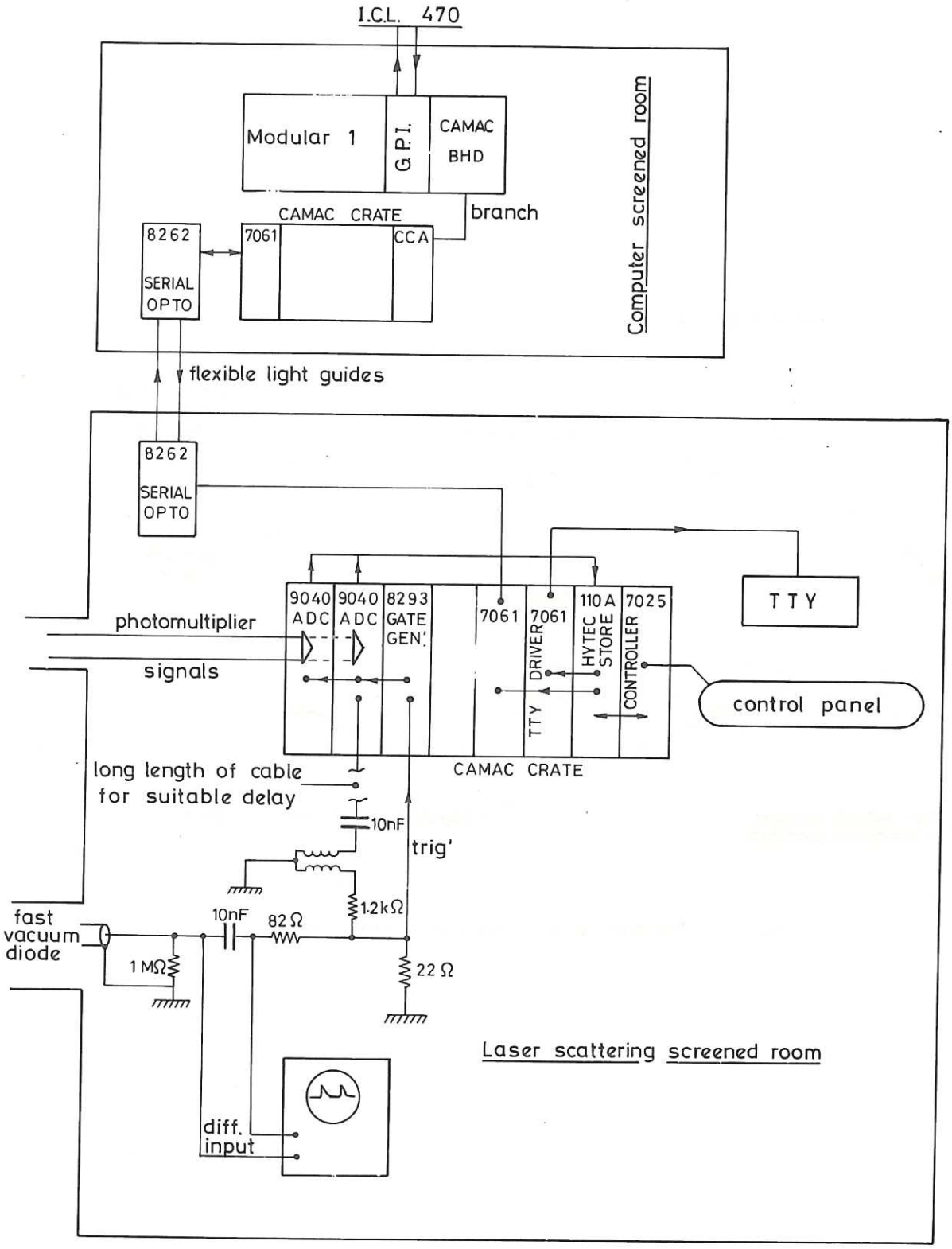

Fig. 9 Schematic of data aquisition system

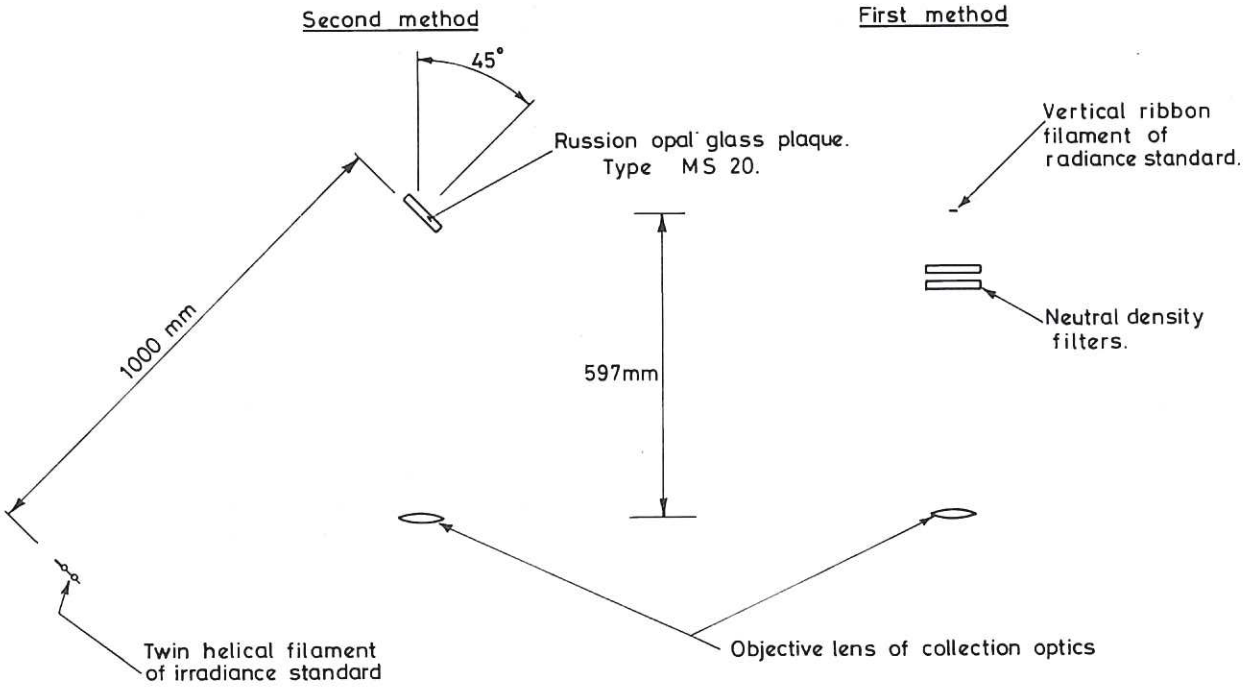

Fig. 10 The alternative standard lamp arrangements.

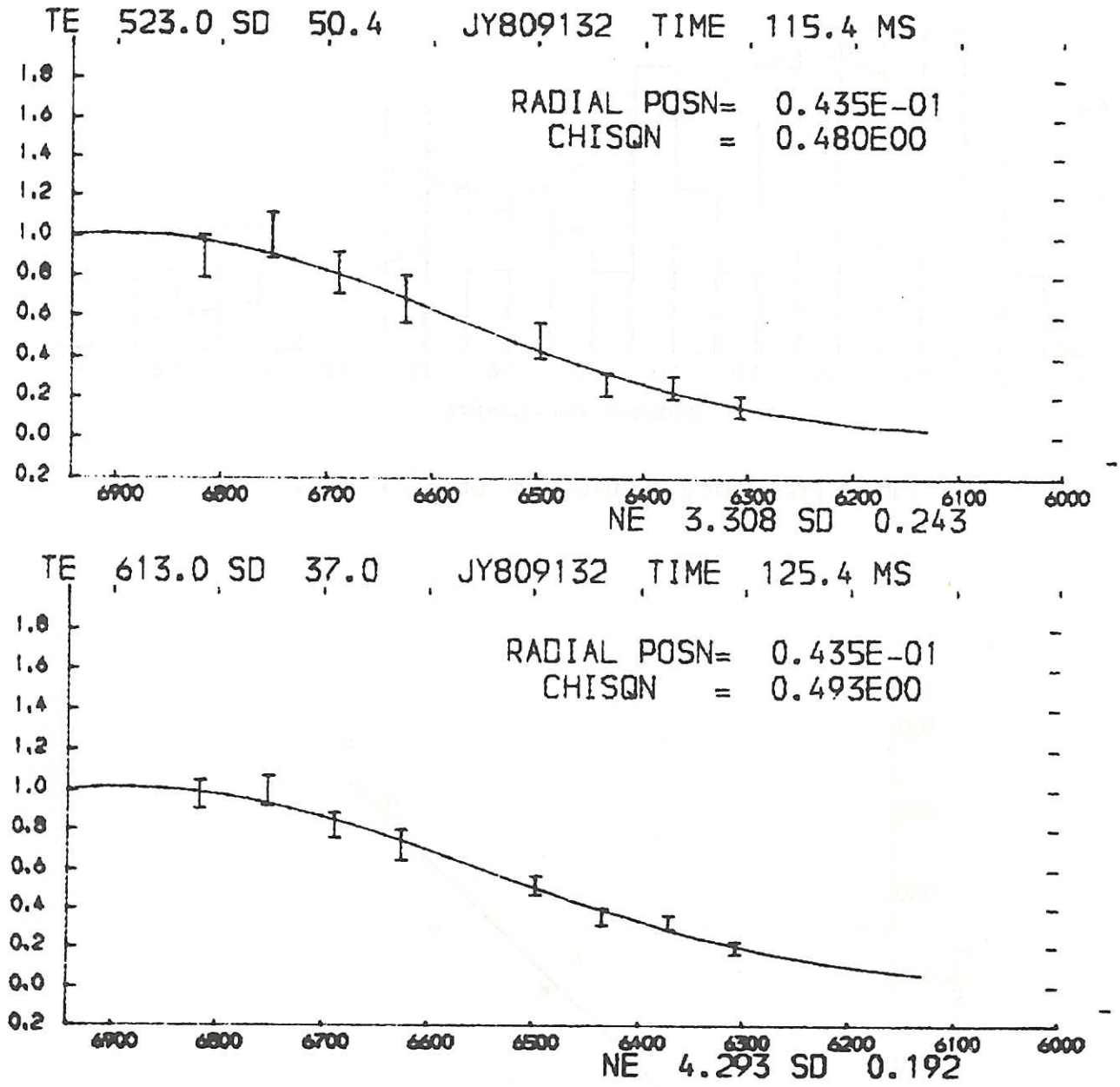
TE 523.0 SD 50.4 JY809132 TIME 115.4 MS
RADIAL POSN= 0.435E-01
CHISQN = 0.480E00
1.8
1.6
1.4
1.2
1.0
0.8
0.6
0.4
0.2
0.0
0.2
6900 6800 6700 6600 6500 6400 6300 6200 6100 6000
NE 3.308 SD 0.243
TE 613.0 SD 37.0 JY809132 TIME 125.4 MS
RADIAL POSN= 0.435E-01
CHISQN = 0.493E00
1.8
1.6
1.4
1.2
1.0
0.8
0.6
0.4
0.2
0.0
0.2
6900 6800 6700 6600 6500 6400 6300 6200 6100 6000
NE 4.293 SD 0.192

Fig. 11

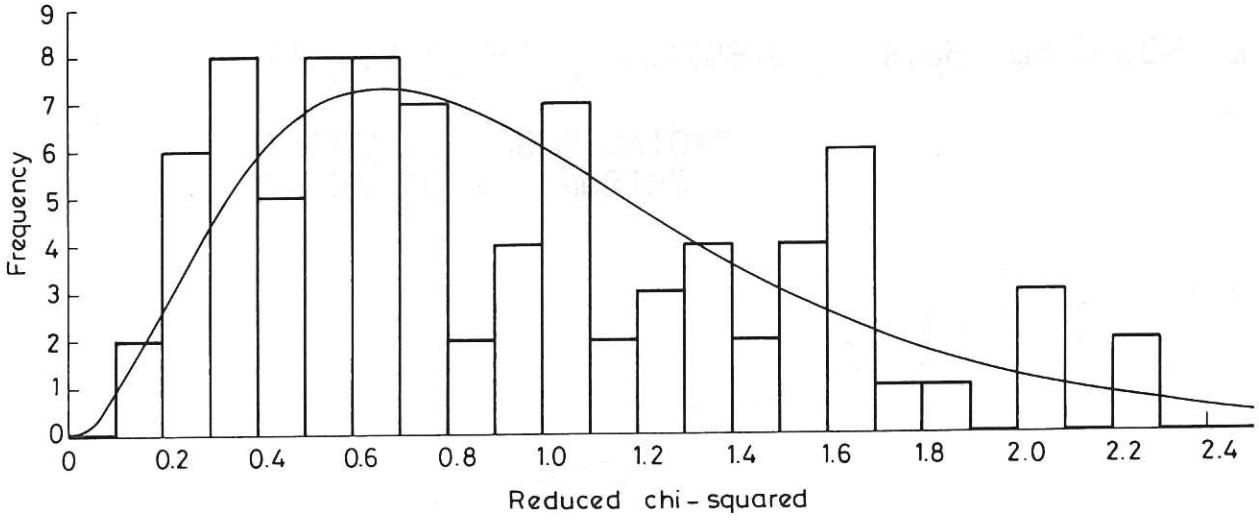

Fig.12 . Frequency distribution of χ^2/ν data

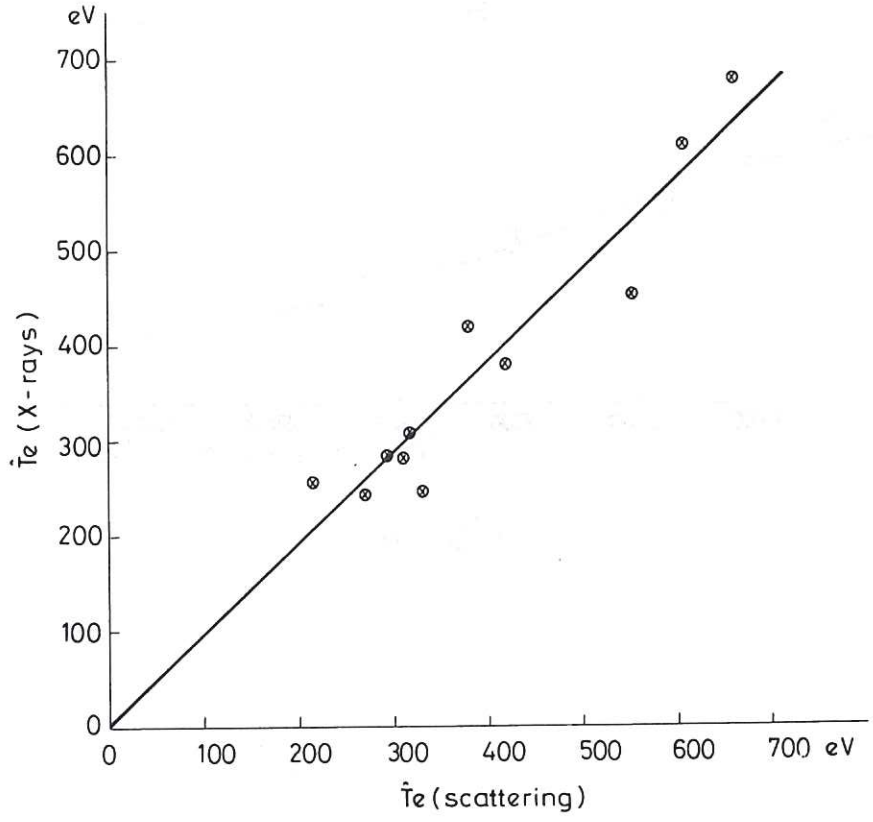

Fig.13. Comparison of X-ray temperature with scattering temperature

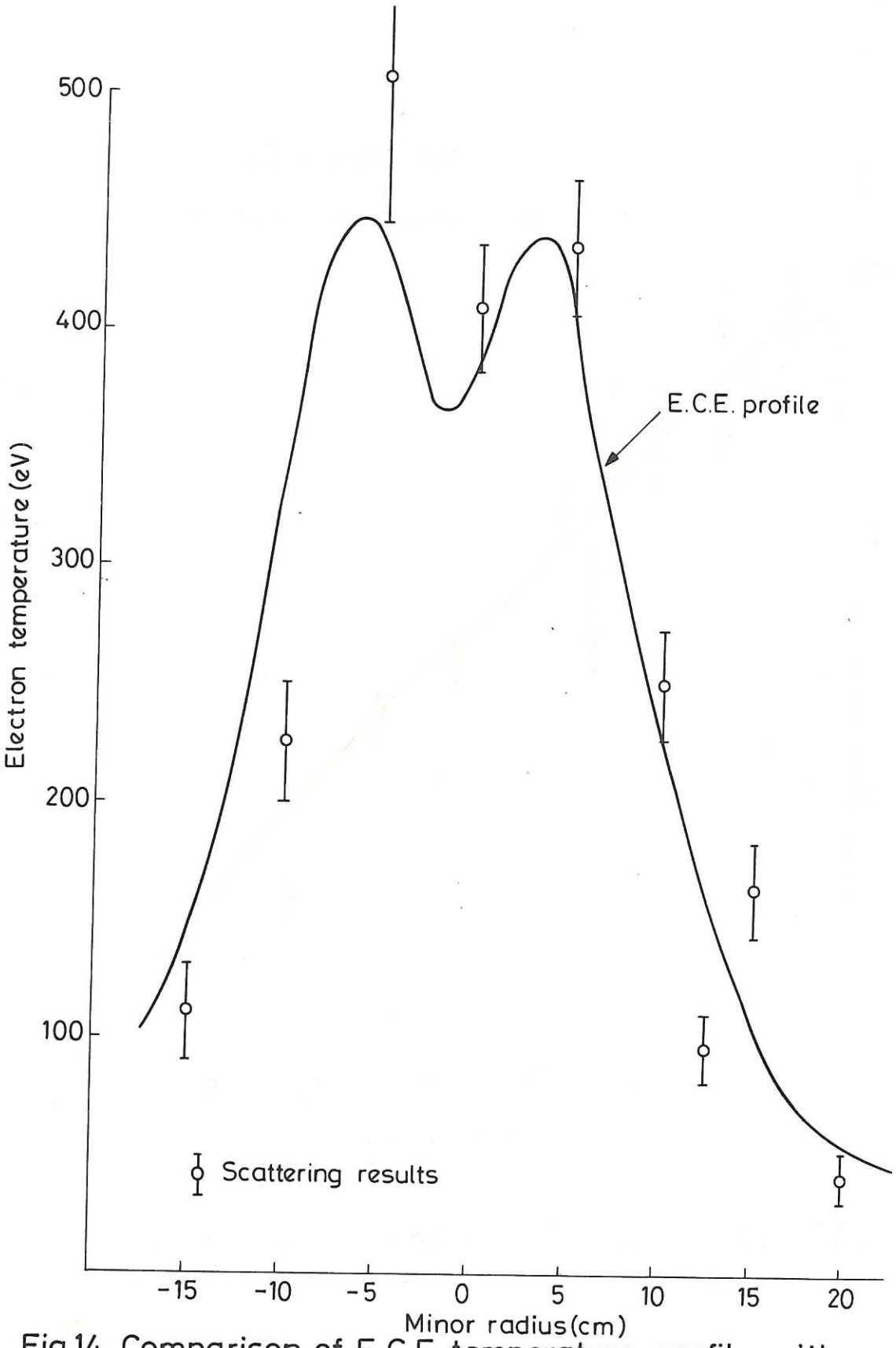

Fig.14. Comparison of E.C.E. temperature profile with scattering profile

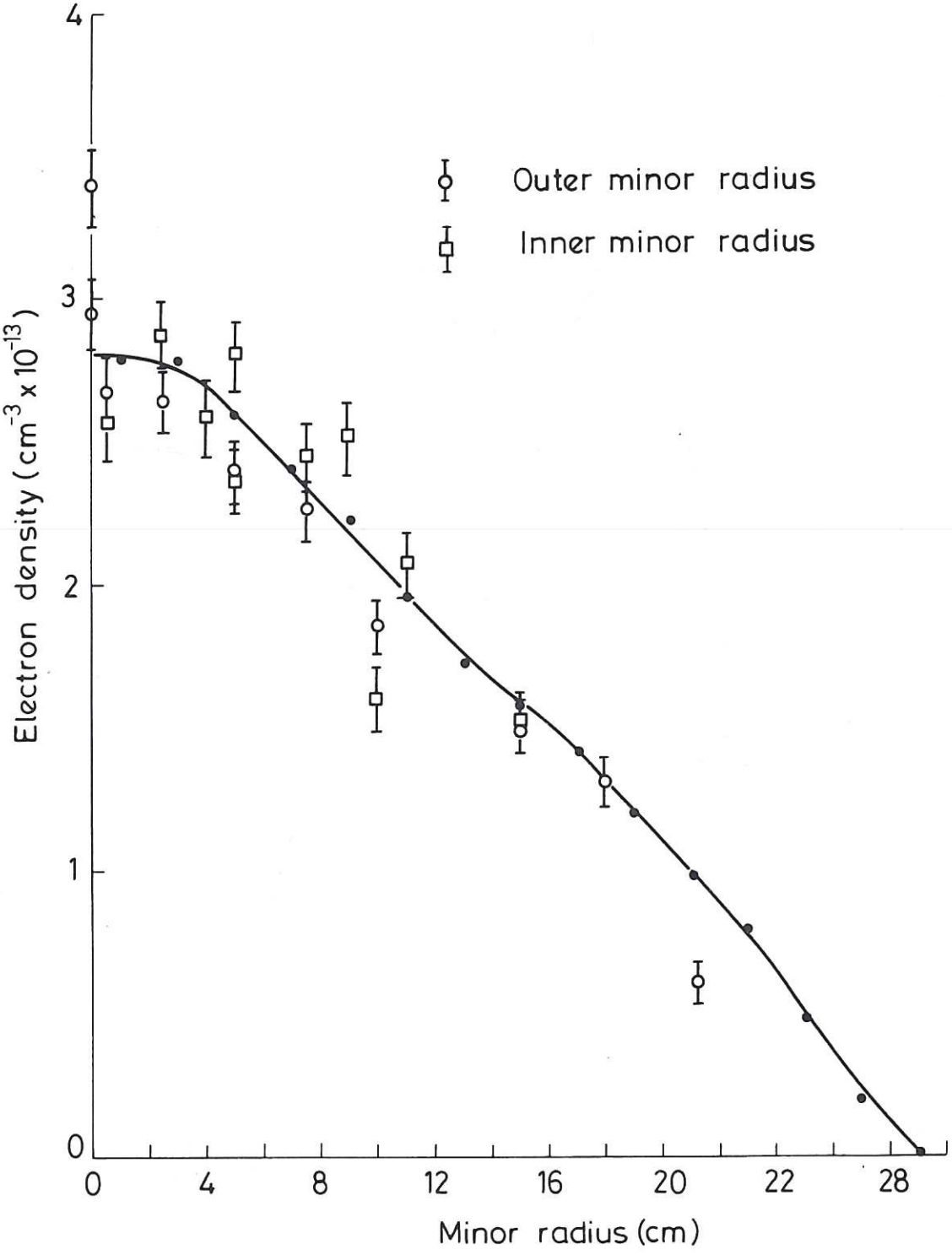

Fig.15. Comparison of microwave interferometer density profile with scattering profile

HER MAJESTY'S STATIONERY OFFICE

Government Bookshops

49 High Holborn, London WC1V 6HB
13a Castle Street, Edinburgh EH2 3AR
41 The Hayes, Cardiff CF1 1JW
Brazennose Street, Manchester M60 8AS
Wine Street, Bristol BS1 2BQ
258 Broad Street, Birmingham B1 2HE
80 Chichester Street, Belfast BT1 4JY

Government publications are also available through booksellers